Hubble Census of Nearby Satellites

Scientific Category:	Stellar Populations and the Interstellar Medium
Alternate Category:	Galaxies
Scientific Keywords:	Dwarf galaxies, Galaxy environments, Galaxy evolution, Globular star clusters, Interacting galaxies, Nearby galaxies, Quenched galaxies, Resolved stellar populations, Star formation histories, Stellar distance
Instruments:	WFC3
Exclusive Access Period:	0 months

Proposal Size: Large	Treasury: Yes	GO-Archival: Yes
Legacy: Yes		

Orbit Request	Prime	Parallel
Cycle 33	149	0

Abstract

Low-mass galaxies provide a crucial means to test the predictions of cosmological models on small scales where they have frequently struggled to match observations. However, the most detailed comparisons have relied almost exclusively on the satellite galaxies in the Local Group (LG) as this was, until recently, the only system with a high level of completeness at low mass and surface brightness. Here we propose a complete census of ALL satellite galaxies (M_V < -9) within MW-like systems out to 10 Mpc. We request 149 orbits to image 149 of these satellites, as well as support to incorporate 111 targets with existing HST observations. Together these observations make up a volume-limited sample of 260 satellites around 22 MW-like hosts. This data set will allow an unbiased characterization of the properties of MW-like satellite systems and end our over-reliance on the LG as the one point of detailed comparison with simulations. Among many other science goals, the observations and analysis that we propose will allow: 1) the most robust measurement of the satellite luminosity function to date, 2) the determination of the globular cluster luminosity function in a lower galaxy mass regime than ever before, and 3) measurements of the star formation histories and quenching times of an unprecedented sample of satellites. Only in the past few years has a project of this scope become possible, as previously the target samples did not exist, and it is only possible with space-based observations. The data products of this program will be fundamental to all studies, both theoretical and observational, of low-mass satellites for the next decade or more.

Target Summary:

Target	RA	Dec	Magnitude
DW0132P1422	01 32 59.6640	+14 22 24.96	V = 16.05
DW0133P1543	01 33 56.2080	+15 43 53.04	V = 19.94
DW0134P1544	01 34 12.8880	+15 44 46.68	V = 17.57
DW0134P1438	01 34 41.7840	+14 38 39.84	V = 17.06
DW0136P1628	01 36 20.2080	+16 28 12.36	V = 17.75
DW0137P1537	01 37 17.6640	+15 37 58.44	V = 17.86
DW0137P1607	01 37 39.7440	+16 07 55.20	V = 20.2
UGC1171	01 39 44.7840	+15 53 57.48	V = 15.71
DW0139P1433	01 39 50.6640	+14 33 22.68	V = 17.89
DW0140P1556	01 40 9.4800	+15 56 21.84	V = 18.64
UGC1176	01 40 10.3200	+15 54 19.44	V = 14.24
DW0143P1541	01 43 36.2880	+15 41 37.32	V = 15.75
DW0141P1651	01 41 40.1520	+16 52 19.56	V = 18.14
DW0221P4221	02 21 12.2400	+42 21 50.40	V = 17.28
UGC1807	02 21 13.3920	+42 45 46.44	V = 13.86
DW0222P4242	02 22 55.1520	+42 42 44.28	V = 17.13
DW0223P4314	02 23 34.1040	+43 14 22.20	V = 19.36
DW0224P4158	02 24 23.2320	+41 58 28.92	V = 20.49
DW0225P4153	02 25 16.6080	+41 53 29.40	V = 20.53
DW0226P4206	02 26 40.5600	+42 06 39.96	V = 20.44
DW0309M4104	03 09 25.1760	-41 04 57.36	V = 19.19
DW0309M4101	03 09 38.2320	-41 01 52.32	V = 12.59
DW0315M4040	03 15 9.7920	-40 40 2.64	V = 18.13
DW0317M4142	03 17 1.4400	-41 42 0.36	V = 16.92
DW0317M4141	03 17 37.9920	-41 41 46.32	V = 17.15
DW0318M4101	03 18 43.1040	-41 01 26.40	V = 18.63
DW0318M4211	03 18 47.0640	-42 11 57.48	V = 20.35
DW0319M4126	03 19 43.3200	-41 26 52.80	V = 17.47
DW0320M4048	03 20 33.8880	-40 48 17.28	V = 19.27
DW0321M4159	03 21 24.5040	-41 59 53.52	V = 16.27
DW0323M4040	03 23 16.1520	-40 40 39.72	V = 15.94
DW0325M4113	03 25 38.3520	-41 13 49.44	V = 17.94
DW0312M3955	03 12 9.1200	-39 55 4.44	V = 20.87
DW0315M4112	03 15 46.1280	-41 12 6.12	V = 20.03
DW0316M4207	03 16 43.6320	-42 07 42.24	V = 20.9
DW0321M4149	03 21 56.4720	-41 49 6.24	V = 20.35

Target	RA	Dec	Magnitude
DW0506M3739	05 06 24.0480	-37 38 59.64	V = 19.83
DW0507M3629	05 07 6.3600	-36 29 0.24	V = 18.73
DW0507M3739	05 07 24.7200	-37 39 6.48	V = 17.84
DW0507M3744	05 07 52.1760	-37 44 18.60	V = 16.92
DW0507M3800	05 07 55.3920	-38 00 45.00	V = 17.96
DW0508M3818	05 08 7.6320	-38 18 35.28	V = 11.81
DW0508M3617	05 08 30.4560	-36 17 12.84	V = 19.47
DW0508M3808	05 08 32.8560	-38 08 25.80	V = 16.82
NGC1827	05 10 4.9920	-36 57 39.96	V = 12.73
DW0502M3845	05 02 33.4560	-38 45 53.64	V = 19.23
DW0506M3800	05 06 8.3040	-38 00 37.08	V = 19.85
DW0507M3733	05 07 29.3760	-37 33 14.76	V = 21.14
DW0848P3226	08 48 39.8400	+32 26 39.12	V = 20.01
DW0853P3318	08 53 26.8080	+33 18 18.72	V = 18.4
DW0855P3336	08 55 10.4640	+33 36 55.80	V = 18.7
DW0856P3155	08 56 25.9200	+31 55 1.92	V = 18.95
DW0929P2213	09 29 54.6480	+22 13 5.16	V = 20.59
DW0930P2143	09 30 39.9840	+21 43 26.40	V = 18.96
DW0932P1952	09 32 23.7840	+19 52 31.44	V = 19.33
DW0933P2030	09 33 13.6560	+20 30 54.72	V = 17.39
DW0936P2135	09 36 21.3840	+21 35 57.48	V = 17.84
DW1042P2415	10 42 21.9840	+24 15 1.80	V = 17.24
DW1042P2501	10 42 43.5600	+25 01 30.00	V = 20.79
DW1045P2427	10 45 31.0320	+24 27 56.52	V = 19.8
DW1044P2610	10 44 29.1120	+26 10 41.52	V = 20.38
DW1119P5543	11 19 48.5520	+55 43 20.64	V = 16.18
DW1108P5520	11 08 59.6160	+55 20 28.32	V = 19.08
DW1109P5447	11 09 13.2000	+54 47 8.16	V = 19.45
DW1110P5429	11 10 35.3040	+54 29 50.28	V = 20.48
DW1111P5631	11 11 47.3280	+56 31 55.20	V = 18.78
DW1111P5547	11 11 56.6160	+55 47 57.48	V = 19.97
DW1113P5529	11 13 7.3200	+55 29 33.36	V = 20.6
DW1113P5541	11 13 10.3200	+55 41 18.96	V = 20.13
DW1113P5644	11 13 35.9040	+56 44 7.80	V = 20.21
DW1116P5551	11 16 7.6080	+55 51 42.12	V = 21.16
DW1220P4729	12 20 30.1440	+47 29 26.16	V = 20.41
DW1220P4649	12 20 54.8640	+46 49 48.72	V = 18.9
DW1223P4739	12 23 46.1760	+47 39 32.04	V = 18.12
DW1223P4644	12 23 49.0080	+46 44 58.20	V = 20.55
DW1227P0136	12 27 46.5120	+01 35 59.28	V = 15.72
DW1232P0015	12 32 36.1200	+00 15 45.00	V = 17.51

Target	RA	Dec	Magnitude
DW1236M0025	12 36 42.1200	-00 25 49.80	V = 18.68
DW1238P0028	12 38 14.0640	+00 28 37.56	V = 19.7
DW1238M0035	12 38 49.2240	-00 35 52.08	V = 19.2
DW1238M0105	12 38 50.0640	-01 05 12.48	V = 20.42
DW1239M0039	12 39 2.5920	-00 39 51.84	V = 16.88
DW1237M1125	12 37 11.6400	-11 25 59.52	V = 18.32
DW1239M1159	12 39 9.0480	-11 59 12.12	V = 19.14
DW1239M1143	12 39 15.2640	-11 43 8.04	V = 16.46
DW1239M1113	12 39 32.7840	-11 13 36.48	V = 18.3
DW1239M1120	12 39 51.4800	-11 20 28.68	V = 19.47
DW1239M1144	12 39 54.8880	-11 44 45.60	V = 17.31
DW1240M1118	12 40 9.4080	-11 18 50.04	V = 15.95
DW1240M1140	12 40 17.5920	-11 40 45.48	V = 18.34
DW1241M1131	12 41 2.8080	-11 31 43.68	V = 19.81
DW1241M1153	12 41 12.0480	-11 53 29.76	V = 18.33
DW1241M1155	12 41 18.7440	-11 55 31.44	V = 17.5
DW1238M1122	12 38 33.6480	-11 22 5.16	V = 17.58
DW1238M1102	12 38 58.2960	-11 02 9.60	V = 20.78
DW1242M1116	12 42 43.8000	-11 16 26.04	V = 17.94
DW1242M1129	12 42 49.6080	-11 29 21.48	V = 21.17
DW1239P3230	12 39 5.1120	+32 30 16.56	V = 18.27
DW1239P3251	12 39 19.6080	+32 51 38.88	V = 20.25
DW1240P3216	12 40 53.0160	+32 16 55.92	V = 18.98
DW1240P3247	12 40 58.4880	+32 47 25.44	V = 16.32
DW1241P3251	12 41 47.1360	+32 51 27.72	V = 15.71
DW1242P3237	12 42 6.1200	+32 37 18.84	V = 19.16
DW1242P3158	12 42 31.3920	+31 58 9.12	V = 19.2
DW1247P3313	12 47 37.9920	+33 13 59.16	V = 20.24
DW1249P4421	12 49 31.1280	+44 21 34.20	V = 16.9
DW1251P4138	12 51 4.7520	+41 38 7.08	V = 18.45
DW1255P4035	12 55 2.7600	+40 35 24.72	V = 18.79
DW1241P4103	12 41 0.9600	+41 03 10.80	V = 18.86
DW1242P4115	12 42 11.3040	+41 15 9.00	V = 18.25
DW1303P4222	13 03 14.3280	+42 22 23.88	V = 17.88
DW1305P4206	13 05 59.7600	+42 06 22.32	V = 18.42
DW1308P4054	13 08 45.9120	+40 54 3.60	V = 17.94
UGC7929	12 45 20.7840	+21 25 37.56	V = 15.93
DW1258P2329	12 58 51.3360	+23 29 23.64	V = 19.14
DW1300P1843	13 00 31.0800	+18 43 3.72	V = 17.89
DW1251P2324	12 51 28.3920	+23 24 3.24	V = 19.12
DW1310P4153	13 10 41.8320	+41 53 26.88	V = 19.12

Target	RA	Dec	Magnitude
DW1312P4158	13 12 18.5280	+41 58 31.80	V = 19.62
UGCA337	13 12 58.5600	+41 47 11.04	V = 15.25
UGC8313	13 13 54.0960	+42 12 33.12	V = 14.12
DW1315P4123	13 15 15.7920	+41 23 48.12	V = 20.71
DW1315P4130	13 15 29.8080	+41 30 7.92	V = 17.67
DW1321P4226	13 21 28.9920	+42 26 0.24	V = 20.11
DW1305P4206-N2	13 05 59.7600	+42 06 22.32	V = 18.42
DW1308P4054-N2	13 08 45.9120	+40 54 3.60	V = 17.95
DW1315P4304	13 15 0.5040	+43 05 5.64	V = 18.97
DW1323-40B	13 24 0.0000	-40 50 12.12	V = 18.52
DW1323-40	13 24 58.1040	-40 45 43.92	V = 18.2
DW1329-45	13 29 14.9040	-45 10 36.12	V = 18.4
CENA-MM-DW9	13 33 1.0080	-42 31 48.00	V = 18.59
CENA-MM-DW8	13 33 34.0080	-41 36 28.08	V = 17.42
DW1336-44	13 36 48.7920	-43 51 28.08	V = 18.7
DW1341-43	13 41 36.6000	-43 51 19.44	V = 17.17
DW1330P4731	13 30 33.8640	+47 31 32.52	V = 20.54
DW1340-30	13 40 19.0080	-30 21 34.92	V = 19.12
DW1350P5441	13 50 58.3440	+54 41 21.12	V = 17.2
UGC8882	13 57 14.6880	+54 06 2.88	V = 14.96
DW1905M6316	19 05 55.9440	-63 16 19.56	V = 18.32
DW1906M6357	19 06 57.9600	-63 57 48.96	V = 16.43
DW1907M6342	19 07 22.5360	-63 42 23.04	V = 17.88
DW1908M6343	19 08 43.9200	-63 43 48.36	V = 14.55
DW1859M6402	18 59 26.5200	-64 02 22.56	V = 19.67
DW1901M6315	19 01 29.5680	-63 15 33.84	V = 17.96
DW1903M6449	19 03 22.3200	-64 49 39.72	V = 19.44
DW1903M6405	19 03 39.5040	-64 05 54.60	V = 20.39
DW1909M6341	19 09 8.3280	-63 41 7.08	V = 17.9
DW1912M6432	19 12 22.8720	-64 32 30.84	V = 19.68
DW1048P1239	10 48 35.9000	+12 39 21.00	V = 16.91

Observing Summary:

Target	Config Mode and Spectral Elements	Flags	Orbits
DW0132P1422	WFC3/UVIS Imaging F814W		1
	WFC3/UVIS Imaging F606W		
DW0133P1543	WFC3/UVIS Imaging F814W	ORIENT	1

Target	Config Mode and Spectral Elements	Flags	Orbits
	WFC3/UVIS Imaging F606W		
DW0134P1544	WFC3/UVIS Imaging F814W	ORIENT	1
	WFC3/UVIS Imaging F606W		
DW0134P1438	WFC3/UVIS Imaging F814W		1
	WFC3/UVIS Imaging F606W		
DW0136P1628	WFC3/UVIS Imaging F814W		1
	WFC3/UVIS Imaging F606W		
DW0137P1537	WFC3/UVIS Imaging F814W		1
	WFC3/UVIS Imaging F606W		
DW0137P1607	WFC3/UVIS Imaging F814W		1
	WFC3/UVIS Imaging F606W		
UGC1171	WFC3/UVIS Imaging F814W		1
	WFC3/UVIS Imaging F606W		
DW0139P1433	WFC3/UVIS Imaging F814W		1
	WFC3/UVIS Imaging F606W		
DW0140P1556	WFC3/UVIS Imaging F814W	ORIENT	1
	WFC3/UVIS Imaging F606W		
UGC1176	WFC3/UVIS Imaging F814W		1
	WFC3/UVIS Imaging F606W		
DW0143P1541	WFC3/UVIS Imaging F814W		1
	WFC3/UVIS Imaging F606W		
DW0141P1651	WFC3/UVIS Imaging F814W		1
	WFC3/UVIS Imaging F606W		
DW0221P4221	WFC3/UVIS Imaging F814W	ORIENT	1
	WFC3/UVIS Imaging F606W		
UGC1807	WFC3/UVIS Imaging F814W	ORIENT	1
	WFC3/UVIS Imaging F606W		
DW0222P4242	WFC3/UVIS Imaging F814W		1
	WFC3/UVIS Imaging F606W		
DW0223P4314	WFC3/UVIS Imaging F814W		1
	WFC3/UVIS Imaging F606W		
DW0224P4158	WFC3/UVIS Imaging F814W		1
	WFC3/UVIS Imaging F606W		
DW0225P4153	WFC3/UVIS Imaging F814W	ORIENT	1
	WFC3/UVIS Imaging F606W		
DW0226P4206	WFC3/UVIS Imaging F814W		1
	WFC3/UVIS Imaging F606W		
DW0309M4104	WFC3/UVIS Imaging F814W	ORIENT	1
	WFC3/UVIS Imaging F606W		
DW0309M4101	WFC3/UVIS Imaging F814W		1
	WFC3/UVIS Imaging F606W		

Target	Config Mode and Spectral Elements	Flags	Orbits
DW0315M4040	WFC3/UVIS Imaging F814W		1
	WFC3/UVIS Imaging F606W		
DW0317M4142	WFC3/UVIS Imaging F814W	ORIENT	1
	WFC3/UVIS Imaging F606W		
DW0317M4141	WFC3/UVIS Imaging F814W		1
	WFC3/UVIS Imaging F606W		
DW0318M4101	WFC3/UVIS Imaging F814W		1
	WFC3/UVIS Imaging F606W		
DW0318M4211	WFC3/UVIS Imaging F814W	ORIENT	1
	WFC3/UVIS Imaging F606W		
DW0319M4126	WFC3/UVIS Imaging F814W		1
	WFC3/UVIS Imaging F606W		
DW0320M4048	WFC3/UVIS Imaging F814W	ORIENT	1
	WFC3/UVIS Imaging F606W		
DW0321M4159	WFC3/UVIS Imaging F814W		1
	WFC3/UVIS Imaging F606W		
DW0323M4040	WFC3/UVIS Imaging F814W		1
	WFC3/UVIS Imaging F606W		
DW0325M4113	WFC3/UVIS Imaging F814W	ORIENT	1
	WFC3/UVIS Imaging F606W		
DW0312M3955	WFC3/UVIS Imaging F814W	ORIENT	1
	WFC3/UVIS Imaging F606W		
DW0315M4112	WFC3/UVIS Imaging F814W		1
	WFC3/UVIS Imaging F606W		
DW0316M4207	WFC3/UVIS Imaging F814W	ORIENT	1
	WFC3/UVIS Imaging F606W		
DW0321M4149	WFC3/UVIS Imaging F814W		1
	WFC3/UVIS Imaging F606W		
DW0506M3739	WFC3/UVIS Imaging F814W	ORIENT	1
	WFC3/UVIS Imaging F606W		
DW0507M3629	WFC3/UVIS Imaging F814W	ORIENT	1
	WFC3/UVIS Imaging F606W		
DW0507M3739	WFC3/UVIS Imaging F814W	ORIENT	1
	WFC3/UVIS Imaging F606W		
DW0507M3744	WFC3/UVIS Imaging F814W	ORIENT	1
	WFC3/UVIS Imaging F606W		
DW0507M3800	WFC3/UVIS Imaging F814W		1
	WFC3/UVIS Imaging F606W		
DW0508M3818	WFC3/UVIS Imaging F814W		1
	WFC3/UVIS Imaging F606W		
DW0508M3617	WFC3/UVIS Imaging F814W	ORIENT	1

Target	Config Mode and Spectral Elements	Flags	Orbits
	WFC3/UVIS Imaging F606W		
DW0508M3808	WFC3/UVIS Imaging F814W	ORIENT	1
	WFC3/UVIS Imaging F606W		
NGC1827	WFC3/UVIS Imaging F814W		1
	WFC3/UVIS Imaging F606W		
DW0502M3845	WFC3/UVIS Imaging F814W		1
	WFC3/UVIS Imaging F606W		
DW0506M3800	WFC3/UVIS Imaging F814W	ORIENT	1
	WFC3/UVIS Imaging F606W		
DW0507M3733	WFC3/UVIS Imaging F814W	ORIENT	1
	WFC3/UVIS Imaging F606W		
DW0848P3226	WFC3/UVIS Imaging F814W	ORIENT	1
	WFC3/UVIS Imaging F606W		
DW0853P3318	WFC3/UVIS Imaging F814W	ORIENT	1
	WFC3/UVIS Imaging F606W		
DW0855P3336	WFC3/UVIS Imaging F814W		1
	WFC3/UVIS Imaging F606W		
DW0856P3155	WFC3/UVIS Imaging F814W		1
	WFC3/UVIS Imaging F606W		
DW0929P2213	WFC3/UVIS Imaging F814W		1
	WFC3/UVIS Imaging F606W		
DW0930P2143	WFC3/UVIS Imaging F814W		1
	WFC3/UVIS Imaging F606W		
DW0932P1952	WFC3/UVIS Imaging F814W	ORIENT	1
	WFC3/UVIS Imaging F606W		
DW0933P2030	WFC3/UVIS Imaging F814W	ORIENT	1
	WFC3/UVIS Imaging F606W		
DW0936P2135	WFC3/UVIS Imaging F814W		1
	WFC3/UVIS Imaging F606W		
DW1042P2415	WFC3/UVIS Imaging F814W	ORIENT	1
	WFC3/UVIS Imaging F606W		
DW1042P2501	WFC3/UVIS Imaging F814W		1
	WFC3/UVIS Imaging F606W		
DW1045P2427	WFC3/UVIS Imaging F814W	ORIENT	1
	WFC3/UVIS Imaging F606W		
DW1044P2610	WFC3/UVIS Imaging F814W	ORIENT	1
	WFC3/UVIS Imaging F606W		
DW1119P5543	WFC3/UVIS Imaging F814W		1
	WFC3/UVIS Imaging F606W		
DW1108P5520	WFC3/UVIS Imaging F814W		1
	WFC3/UVIS Imaging F606W		

Target	Config Mode and Spectral Elements	Flags	Orbits
DW1109P5447	WFC3/UVIS Imaging F814W		1
	WFC3/UVIS Imaging F606W		
DW1110P5429	WFC3/UVIS Imaging F814W		1
	WFC3/UVIS Imaging F606W		
DW1111P5631	WFC3/UVIS Imaging F814W	ORIENT	1
	WFC3/UVIS Imaging F606W		
DW1111P5547	WFC3/UVIS Imaging F814W	ORIENT	1
	WFC3/UVIS Imaging F606W		
DW1113P5529	WFC3/UVIS Imaging F814W	ORIENT	1
	WFC3/UVIS Imaging F606W		
DW1113P5541	WFC3/UVIS Imaging F814W		1
	WFC3/UVIS Imaging F606W		
DW1113P5644	WFC3/UVIS Imaging F814W		1
	WFC3/UVIS Imaging F606W		
DW1116P5551	WFC3/UVIS Imaging F814W		1
	WFC3/UVIS Imaging F606W		
DW1220P4729	WFC3/UVIS Imaging F814W	ORIENT	1
	WFC3/UVIS Imaging F606W		
DW1220P4649	WFC3/UVIS Imaging F814W		1
	WFC3/UVIS Imaging F606W		
DW1223P4739	WFC3/UVIS Imaging F814W		1
	WFC3/UVIS Imaging F606W		
DW1223P4644	WFC3/UVIS Imaging F814W		1
	WFC3/UVIS Imaging F606W		
DW1227P0136	WFC3/UVIS Imaging F814W		1
	WFC3/UVIS Imaging F606W		
DW1232P0015	WFC3/UVIS Imaging F814W		1
	WFC3/UVIS Imaging F606W		
DW1236M0025	WFC3/UVIS Imaging F814W	ORIENT	1
	WFC3/UVIS Imaging F606W		
DW1238P0028	WFC3/UVIS Imaging F814W	ORIENT	1
	WFC3/UVIS Imaging F606W		
DW1238M0035	WFC3/UVIS Imaging F814W		1
	WFC3/UVIS Imaging F606W		
DW1238M0105	WFC3/UVIS Imaging F814W	ORIENT	1
	WFC3/UVIS Imaging F606W		
DW1239M0039	WFC3/UVIS Imaging F814W		1
	WFC3/UVIS Imaging F606W		
DW1237M1125	WFC3/UVIS Imaging F814W	ORIENT	1
	WFC3/UVIS Imaging F606W		
DW1239M1159	WFC3/UVIS Imaging F814W		1

Target	Config Mode and Spectral Elements	Flags	Orbits
	WFC3/UVIS Imaging F606W		
DW1239M1143	WFC3/UVIS Imaging F814W	ORIENT	1
	WFC3/UVIS Imaging F606W		
DW1239M1113	WFC3/UVIS Imaging F814W		1
	WFC3/UVIS Imaging F606W		
DW1239M1120	WFC3/UVIS Imaging F814W		1
	WFC3/UVIS Imaging F606W		
DW1239M1144	WFC3/UVIS Imaging F814W		1
	WFC3/UVIS Imaging F606W		
DW1240M1118	WFC3/UVIS Imaging F814W	ORIENT	1
	WFC3/UVIS Imaging F606W		
DW1240M1140	WFC3/UVIS Imaging F814W	ORIENT	1
	WFC3/UVIS Imaging F606W		
DW1241M1131	WFC3/UVIS Imaging F814W	ORIENT	1
	WFC3/UVIS Imaging F606W		
DW1241M1153	WFC3/UVIS Imaging F814W	ORIENT	1
	WFC3/UVIS Imaging F606W		
DW1241M1155	WFC3/UVIS Imaging F814W		1
	WFC3/UVIS Imaging F606W		
DW1238M1122	WFC3/UVIS Imaging F814W	ORIENT	1
	WFC3/UVIS Imaging F606W		
DW1238M1102	WFC3/UVIS Imaging F814W		1
	WFC3/UVIS Imaging F606W		
DW1242M1116	WFC3/UVIS Imaging F814W		1
	WFC3/UVIS Imaging F606W		
DW1242M1129	WFC3/UVIS Imaging F814W	ORIENT	1
	WFC3/UVIS Imaging F606W		
DW1239P3230	WFC3/UVIS Imaging F814W		1
	WFC3/UVIS Imaging F606W		
DW1239P3251	WFC3/UVIS Imaging F814W	ORIENT	1
	WFC3/UVIS Imaging F606W		
DW1240P3216	WFC3/UVIS Imaging F814W		1
	WFC3/UVIS Imaging F606W		
DW1240P3247	WFC3/UVIS Imaging F814W		1
	WFC3/UVIS Imaging F606W		
DW1241P3251	WFC3/UVIS Imaging F814W		1
	WFC3/UVIS Imaging F606W		
DW1242P3237	WFC3/UVIS Imaging F814W	ORIENT	1
	WFC3/UVIS Imaging F606W		
DW1242P3158	WFC3/UVIS Imaging F814W		1
	WFC3/UVIS Imaging F606W		

Target	Config Mode and Spectral Elements	Flags	Orbits
DW1247P3313	WFC3/UVIS Imaging F814W		1
	WFC3/UVIS Imaging F606W		
DW1249P4421	WFC3/UVIS Imaging F814W	ORIENT	1
	WFC3/UVIS Imaging F606W		
DW1251P4138	WFC3/UVIS Imaging F814W	ORIENT	1
	WFC3/UVIS Imaging F606W		
DW1255P4035	WFC3/UVIS Imaging F814W		1
	WFC3/UVIS Imaging F606W		
DW1241P4103	WFC3/UVIS Imaging F814W		1
	WFC3/UVIS Imaging F606W		
DW1242P4115	WFC3/UVIS Imaging F814W	ORIENT	1
	WFC3/UVIS Imaging F606W		
DW1303P4222	WFC3/UVIS Imaging F814W		1
	WFC3/UVIS Imaging F606W		
DW1305P4206	WFC3/UVIS Imaging F814W		1
	WFC3/UVIS Imaging F606W		
DW1308P4054	WFC3/UVIS Imaging F814W	ORIENT	1
	WFC3/UVIS Imaging F606W		
UGC7929	WFC3/UVIS Imaging F814W		1
	WFC3/UVIS Imaging F606W		
DW1258P2329	WFC3/UVIS Imaging F814W		1
	WFC3/UVIS Imaging F606W		
DW1300P1843	WFC3/UVIS Imaging F814W		1
	WFC3/UVIS Imaging F606W		
DW1251P2324	WFC3/UVIS Imaging F814W		1
	WFC3/UVIS Imaging F606W		
DW1310P4153	WFC3/UVIS Imaging F814W		1
	WFC3/UVIS Imaging F606W		
DW1312P4158	WFC3/UVIS Imaging F814W		1
	WFC3/UVIS Imaging F606W		
UGCA337	WFC3/UVIS Imaging F814W	ORIENT	1
	WFC3/UVIS Imaging F606W		
UGC8313	WFC3/UVIS Imaging F814W		1
	WFC3/UVIS Imaging F606W		
DW1315P4123	WFC3/UVIS Imaging F814W		1
	WFC3/UVIS Imaging F606W		
DW1315P4130	WFC3/UVIS Imaging F814W		1
	WFC3/UVIS Imaging F606W		
DW1321P4226	WFC3/UVIS Imaging F814W		1
	WFC3/UVIS Imaging F606W		
DW1305P4206-N2	WFC3/UVIS Imaging F814W		1

Target	Config Mode and Spectral Elements	Flags	Orbits
	WFC3/UVIS Imaging F606W		
DW1308P4054-N2	WFC3/UVIS Imaging F814W		1
	WFC3/UVIS Imaging F606W		
DW1315P4304	WFC3/UVIS Imaging F814W		1
	WFC3/UVIS Imaging F606W		
DW1323-40B	WFC3/UVIS Imaging F814W	ORIENT	1
	WFC3/UVIS Imaging F606W		
DW1323-40	WFC3/UVIS Imaging F814W	ORIENT	1
	WFC3/UVIS Imaging F606W		
DW1329-45	WFC3/UVIS Imaging F814W	ORIENT	1
	WFC3/UVIS Imaging F606W		
CENA-MM-DW9	WFC3/UVIS Imaging F814W		1
	WFC3/UVIS Imaging F606W		
CENA-MM-DW8	WFC3/UVIS Imaging F814W		1
	WFC3/UVIS Imaging F606W		
DW1336-44	WFC3/UVIS Imaging F814W	ORIENT	1
	WFC3/UVIS Imaging F606W		
DW1341-43	WFC3/UVIS Imaging F814W	ORIENT	1
	WFC3/UVIS Imaging F606W		
DW1330P4731	WFC3/UVIS Imaging F814W		1
	WFC3/UVIS Imaging F606W		
DW1340-30	WFC3/UVIS Imaging F814W	ORIENT	1
	WFC3/UVIS Imaging F606W		
DW1350P5441	WFC3/UVIS Imaging F814W		1
	WFC3/UVIS Imaging F606W		
UGC8882	WFC3/UVIS Imaging F814W		1
	WFC3/UVIS Imaging F606W		
DW1905M6316	WFC3/UVIS Imaging F814W		1
	WFC3/UVIS Imaging F606W		
DW1906M6357	WFC3/UVIS Imaging F814W	ORIENT	1
	WFC3/UVIS Imaging F606W		
DW1907M6342	WFC3/UVIS Imaging F814W		1
	WFC3/UVIS Imaging F606W		
DW1908M6343	WFC3/UVIS Imaging F814W		1
	WFC3/UVIS Imaging F606W		
DW1859M6402	WFC3/UVIS Imaging F814W	ORIENT	1
	WFC3/UVIS Imaging F606W		
DW1901M6315	WFC3/UVIS Imaging F814W	ORIENT	1
	WFC3/UVIS Imaging F606W		
DW1903M6449	WFC3/UVIS Imaging F814W	ORIENT	1
	WFC3/UVIS Imaging F606W		

Target	Config Mode and Spectral Elements	Flags	Orbits
DW1903M6405	WFC3/UVIS Imaging F814W	ORIENT	1
	WFC3/UVIS Imaging F606W		
DW1909M6341	WFC3/UVIS Imaging F814W		1
	WFC3/UVIS Imaging F606W		
DW1912M6432	WFC3/UVIS Imaging F814W	ORIENT	1
	WFC3/UVIS Imaging F606W		
DW1048P1239	WFC3/UVIS Imaging F814W	ORIENT	1
	WFC3/UVIS Imaging F606W		

Total prime orbits: 149

Investigators:

Investigators and Team Expertise are included in this preview for your team to review. These will not appear in the version of the proposal given to the TAC, to allow for a dual anonymous review.

Role		Investigator	Institution	Country
CoI		Dr. Paul Bennet	Space Telescope Science Institute	USA/MD
CoI		Dr. Denija Crnojevic	University of Tampa	USA/FL
CoI	*	Dr. Amandine Doliva-Dolinsky	University of Surrey	GBR
CoI		Dr. Catherine Fielder	University of Arizona	USA/AZ
CoI		Dr. Laura Congreve Hunter	Dartmouth College	USA/NH
PI	&	Dr. Michael Gordon Jones	University of Arizona	USA/AZ
CoI	!	Dr. Ananthan Karunakaran	University of Toronto	CAN
CoI		Donghyeon Khim	University of Arizona	USA/AZ
CoI		Dr. Burcin Mutlu-Pakdil	Dartmouth College	USA/NH
CoI		Dr. Eric W. Peng	NOIRLab - (AZ)	USA/MD
CoI		Dr. Deepthi S. Prabhu	University of Arizona	USA/AZ
CoI		Prof. David J. Sand	University of Arizona	USA/AZ
CoI	!	Dr. Kristine Spekkens	Queen's University	CAN
CoI		Prof. Dennis Zaritsky	University of Arizona	USA/AZ

Number of investigators: 14

* ESA investigators: 1

! CSA investigators: 2

& Contacts: 1

Team Expertise:

M. Jones is an expert in galaxies in the local Universe. He has extensive experience in HI (atomic gas) extragalactic astronomy and has been a member of the ALFALFA team for 10 years. He has led work quantifying the GC systems of ultra-diffuse galaxies, both in group environments (Program ID: 15874, PI: K. Spekkens) and in the field (Program ID: SNAP16758, PI: M. Jones). He has also led the investigation of "blue blobs," a novel class of young star-forming clouds in the Virgo galaxy cluster (Program ID: 15183, PI: D. Sand and Program ID: 17267, PI: M. Jones). He is currently a post-doc at Steward Observatory working with D. Sand.

D. Sand has been a PI or CoI of over 10 successful HST proposals and is an expert in both dwarf galaxies and supernovae. He has extensive experience with HST imaging and has published numerous papers on faint and diffuse dwarf galaxies. He is faculty at Steward Observatory.

P. Bennet is a post-doc at STScI. He has considerable experience working with HST imaging and is an expert in satellite luminosity functions.

D. Crnojevic is faculty at University of Tampa. She has extensive experience of HST imaging and is an expert in faint dwarf galaxies, resolved structures in stellar halos, and measurement of the TRGB from HST imaging.

A. Karunakaran is a post-doc at the University of Toronto. He has led much of the work investigating the quenched fractions of satellite systems in both the ELVES and SAGA samples. He is also an expert in ultra-diffuse galaxies and HI observations.

B. Mutlu-Pakdil is an expert in ultra-faint dwarf galaxies and deep imaging. She has extensive experience with HST imaging. She is faculty at Darthmouth College.

K. Spekkens is faculty at the Royal Military College of Canada and Queen's University. She is an expert in the kinematics and structure of galactic disks.

C. Fielder is an expert in the spectral energy distribution of Milky Way-like galaxies and has lef work studying the globular cluster populations of ultra-diffuse galaxies observed with HST (Program ID: 16890, PI: D. Sand). She is a post-doc at Steward Observatory.

D. Zaritsky is faculty at the University of Arizona and is an expert in numerous areas of extragalactic astronomy, including low surface brightness galaxies. He is also has extensive experience with the StarFISH CMD fitting code.

A. Doliva-Dolinsky is an expert on faint dwarf galaxies and global properties of satellite systems. She is a postdoctoral researcher at the University of Tampa.

L. Hunter is currently working on identifying some of the faintest satellite galaxies around dwarf galaxy hosts in the Local Volume. She is a post-doctoral researcher at Dartmouth College.

D. Prabhu is a post-doc at the University of Arzona and is an expert in the stellar populations of star clusters.

D. Khim is a graduate student working with D. Zaritsky at the University of Arizona. He has experience with low surface brightness galaxies, in particular ultra-diffuse galaxies.

E. Peng is an astronomer at NOIRLab and an expert in the globular cluster systems of galaxies. He led much of the seminal on globular clusters from the ACS Virgo Cluster, among many other projects.

Scientific Justification

How did the Local Group form and how typical is it when compared to other systems of similar mass? In the Λ Cold Dark Matter (ΛCDM) cosmological paradigm the Local Group (LG) of galaxies assembled via a hierarchical process, a model that reproduces its broad properties as well as the larger scale structure observed in the universe. The low-mass satellite galaxies in such systems are the most dark matter-dominated galaxies in the universe and are subject to the environmental influence of their host galaxies, simultaneously representing powerful tests of both the dark matter (DM) and baryon physics in cosmological simulations. At these small scales, a series of tensions arose between simulations and observations, such as the "missing satellites problem" [1] and the "cusp-core problem" [2]. Successive improvements to the resolution and baryon physics of simulations, as well as the observational census of the LG, have resolved or indicated potential resolutions to these original small-scale challenges of ΛCDM [3, 4]. However, further discrepancies that are increasingly difficult to explain continue to arise (e.g. [5, 6]). The intrinsic system-to-system scatter means that it is unlikely that the physics underpinning these remaining tensions will be understood by studying the LG in ever increasing detail. Instead, **we must place the Local Group satellites in the full context of other similar mass systems in order to make progress.**

To this end, over the past few years several major efforts have been underway to construct complete and reliable samples of satellites around Milky Way-like hosts in the nearby universe (e.g. [7, 8, 9, 10]). However, performing a census of satellite properties with existing (mostly) ground-based data is not sufficient to address the most challenging questions. To understand the 3D structure of nearby satellite systems, the star formation histories (SFHs) of their constituent satellites, as well as to accurately trace their luminosity functions (LFs) and globular cluster properties, space telescope observations are required.

This proposal: **In this GO-AR Treasury proposal we target *all* 260 satellites** ($M_V < -9$) **around MW-like hosts beyond the LG and within 10 Mpc** (Fig. 1), to perform the **Hubble Census of Nearby Satellites** (HCNS). By observing the 149 satellites without existing archival HST observations, HCNS will provide **an unbiased characterization of satellite properties in MW-mass systems**, greatly expanding the current sample size and completeness, as well as the range of satellite environments covered (Fig. 1). This unprecedented and homogeneous census of all Local Volume satellites represents a rich legacy data set suitable for tackling ΛCDM's most significant remaining (and future) small-scale problems. The **GO-AR category is designed for exactly this situation** where only through the combined analysis of new and archival observations can the end science goals be reached. HCNS will: **1)** measure precise distances to all 260 satellites, enabling the most robust measurement of the satellite LF beyond the LG to date, **2)** robustly measure the globular cluster luminosity function (GCLF) in a dwarf galaxy mass regime never before probed from space with a statistical sample, and **3)** enable the analysis of the SFHs and quenching times of an unprecedented number of low-mass satellites spanning a wider range of environments than ever before. HCNS will provide enormous legacy value for all studies, both theoretical and observational, of low-mass satellites for the next decade or more.

Sample selection: Until recently the LG was the only relatively complete sample of low-mass satellites around a MW-mass galaxy. The Exploration of Local VolumE Satellites (ELVES [10]) survey took a major step forward, constructing a nearly volume-limited sample of satellites ($M_V < -9$) around *all* MW-like hosts ($M_{K_s} < -22.1$) out to a distance of 12 Mpc using deep ground-based imaging. The sample is complete to low surface brightness ($\mu_V < 26.5$ mag arcsec^{-2}) and host–satellite associations were determined with (mostly) surface brightness fluctuations (SBF) distance measurements. Although there are archival HST observations of ∼40% of the ELVES sample, these **are highly incomplete and systematically biased towards higher luminosity and higher surface brightness satellites**. HCNS will target all ELVES systems beyond the LG and within 10 Mpc, the maximum distance where we can determine accurate distances for the faintest satellites. This is a complete ($M_V < -9$) sample of 260 satellite candidates around 22 MW-like galaxies.

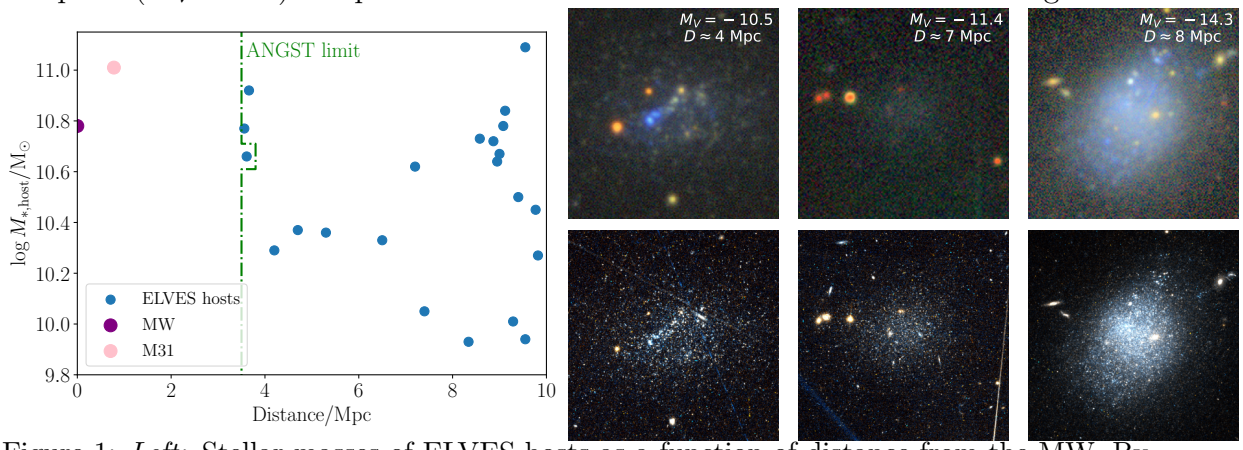

Figure 1: *Left*: Stellar masses of ELVES hosts as a function of distance from the MW. By targeting all systems out to 10 Mpc we will greatly expand the range of satellites environments covered, as well as the statistical power of the sample. The ACS Nearby Galaxy Survey Treasury [11] targeted very nearby galaxies, many of which were not satellites. The overlap is almost all in the M81 system and represents a small, biased sample of satellites. *Right*: Legacy Survey images (top) for a selection of ELVES satellites with archival HST imaging (bottom) that span a representative range of distances and luminosities. The sample includes a broad range of morphologies and surface brightnesses. Each cutout is $50'' \times 50''$.

GOAL 1 - Accurate distances, the satellite luminosity function, and satellite distributions: Over the past decade considerable progress has been made toward resolving the many small-scale problems of ΛCDM that stem from the over-abundance of DM subhalos [4]. However, at the lowest masses such comparisons still mostly rely on a single system of satellites, the LG, an apparent outlier for systems of its mass [6, 12]. ELVES greatly increases the comparison sample for all classical satellites, but distance estimates in this sample rely mostly on SBFs, which are subject to some notable failures (e.g. [13, 14]). Furthermore, the large uncertainty in these distance measurements ($2\sigma \sim 3$ Mpc) leaves considerable room for erroneous associations even when working as intended, and cannot distinguish objects inside/outside the "splashback" radius (∼300 kpc [15]), which is typically used to mark the "edge" of a bound system. Fig. 2 shows the significant potential bias remaining in the satellite LF (at $M_V \gtrsim -14$) as a result of SBF-based host–satellite associations. This is precisely the

regime where ELVES extends beyond the more distant SAGA (Satellites Around Galactic Analogs; [7, 8, 16]) sample as it begins to become incomplete. However, the deviations shown here call into question the reliability of this extension at present. ELVES already includes all nearby MW-like hosts, which are **the only systems where we will have the capability to probe this satellite mass regime in detail for the foreseeable future.** If we want to overcome the uncertainty and bias in Fig. 2 and make robust comparisons to satellite populations in ΛCDM simulations then we require tip of the red giant branch (TRGB) distance measurements. **There will *never* be a sample of closer MW-like systems where this science is possible with current ground-based telescopes.**

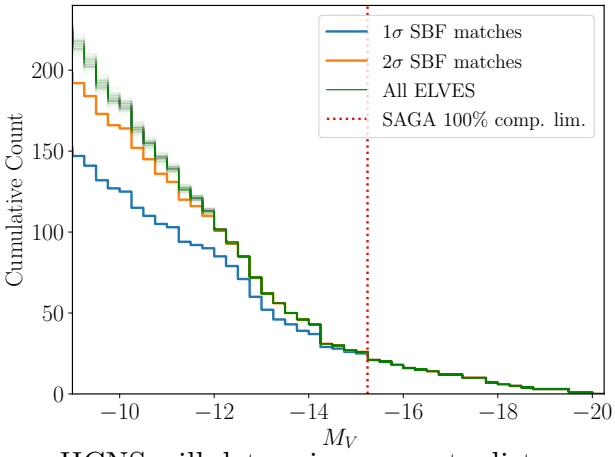

Figure 2: Cumulative satellite LFs for ELVES satellites with SBF distance estimates within 1σ (∼1.5 Mpc) of their putative host (blue line), within 2σ (orange line), and for all satellite candidates (green line). In the last case 200 realizations are plotted based on the probabilities that candidates are associated with their hosts (as given in [10]). At $M_V = -9$ there is up to a 50% uncertainty in the cumulative LF! **Robust TRGB distances are the only means of removing this uncertainty/bias.**

HCNS will determine accurate distances to all 260 targets (new and archival) using the TRGB standard candle. **Our typical expected uncertainty is ∼0.2 Mpc** (cf. [17]), **compared to ∼1.5 Mpc for SBFs** [18]. We note that [19] carried out single-orbit HST/ACS imaging of several ELVES ultra-diffuse galaxies around M96 ($D = 10.7$ Mpc), demonstrating that TRGB distances can be reliably determined for even the faintest satellites at ∼10 Mpc. Of our 22 target systems, only two have no new targets in this proposal, meaning that currently ∼90% do not have robust satellite LF measurements. **Only with *all* satellites confirmed with accurate distances can a robust satellite LF be measured for each host, enabling like-for-like comparisons to the abundance of satellites in simulations** and reliable inferences about the physics driving dwarf galaxy formation.

Robust satellite LFs will also allow examination of recently identified observational relations between the satellite LF, host environment, most massive satellite, and satellite quenched fraction, that are not seen in current simulations [20, 21, 22]. Accurate distances are also essential for robust analysis of the spatial distribution of satellites in these systems. The existence and importance of planes of satellites is still a contentious and hotly debated topic (e.g. [5, 23, 24]), but **some argue that it represents ΛCDM's most significant unresolved small-scale challenge**. There has also been considerable recent interest in the frequency of lopsided satellite distributions (e.g. [25, 23, 26, 27]). For the nearby ($D \lesssim$ 5 Mpc) systems TRGB distances will be accurate enough to determine the 3D configuration of satellites (e.g. [28]), while for the remainder of the sample they will confidently reject any interlopers, after which all remaining candidate planar and lopsided systems can be followed up spectroscopically to confirm if they are kinematically coherent structures (cf. [29, 30, 31]).

GOAL 2 - Globular cluster systems of satellites: Globular clusters (GCs) are signposts for extremely dense SF at high-z, trace the subsequent dynamical evolution of their host galaxies, and hold clues to the underlying structure (cusp vs core) of their DM halos [32, 33]. Zoom-in cosmological simulations are on the cusp of including GCs formation models in simulated galaxies analogous to those in ELVES [34, 35, 36], but without a corresponding robust observational census, these upcoming predictions will remain largely untested. Previous GC censuses have focused on massive galaxies and/or galaxy clusters (e.g. [37, 38, 39, 40, 41, 42]), where environmental process are likely to skew the population. The existing ground-based analysis of the GCs in ELVES [43] has high contamination uncertainties due to inadequate background galaxy separation, overlooks GCs that are clearly visible in archival HST imaging (e.g. CenA-Dw1, [44]), and has an insufficient point source depth to detect faint GCs. **HCNS will perform a complete census of GCs in all 260 satellites, providing the first ever robust statistical sample of GCs for galaxies in this mass range, outside of a galaxy cluster**. GCs have repeatedly been shown to be an excellent proxy for total mass [45, 46, 47, 48], thus by stacking the lowest mass satellites and combining with individual higher mass satellites we will place new constraints on the stellar mass–halo mass relation from sub-halos in MW-like systems down to $M_* \sim 10^6$ $M_\odot$.

The current standard references for the abundance of GCs [46] and the GCLF in dwarf galaxies [49] are both based on compilations of HST observations as these provide by far the most reliable identification of GCs with imaging alone. However, the former effectively ends 3 mag brighter than the limiting absolute magnitude of ELVES, while the latter is based on a sample with a median $M_V \approx -15$ compared to ≈ -11 for ELVES. Based on the hurdle model of [50] we expect to detect on average 1.7 GCs per $M_V > -14$ target (213 satellites; >350 GCs expected). Thus, a large sample (such as HCNS) is essential to construct a GCLF and assess the typical richness of GC systems at these galaxy masses; **such a measurement would constitute a new standard reference for all future studies of dwarf galaxies**. For the 46 brighter satellites we will be able to go beyond global statistics and study the properties of individual GC systems. The discovery (or lack of) GCs near the central regions of low-mass galaxies can place tight constraints on their DM structure. For example, the mere survival of GCs near the center of a dwarf can imply that the halo is cored (rather than cuspy), otherwise dynamical friction would have long ago caused it to in-spiral (e.g. Fornax [51] and Eridanus II [52]). The Fornax dSph has five GCs near its center and has been the subject of extensive theorizing and speculation for two decades (e.g. [53, 54, 55, 56, 57, 58, 59]), but these arguments are inevitably limited by being focused on a single object. Although Fornax is remarkable, the real question is: *How many Fornax's are there?* A question that HCNS will unequivocally answer.

GOAL 3 - Quenching and star formation histories of satellites: Satellite quenching is a crucial process that all star-forming field dwarfs must go through when they fall into a group and become quiescent satellites like those found in the LG [60, 61]. Yet how quenching proceeds in MW-mass groups is still an open question, with the dominant mechanism(s), and the speed at which quenching proceeds, still largely unknown (e.g. [62]). Recent work [63, 6, 12] has shown that star-forming satellites are far more common in other MW-mass

groups than they are around the actual MW or in zoom-in simulations that closely mimic the LG; an issue that is beginning to be referred to as the "satellite quenching problem."

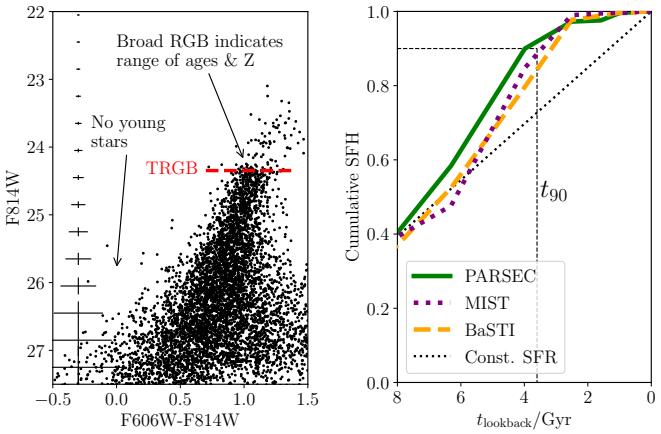

Figure 3: *Left*: CMD of dwarf satellite IC4107 ($D = 4.8$ Mpc) from a single-orbit archival observation. The TRGB is clearly visible. Photometric uncertainties from artificial stars are shown by errorbars on the left. *Right*: Cumulative SFH fit to the CMD (see Desc. of Obs.). Three colored lines show the SFH based on different stellar isochrone libraries [64, 65, 66]. All agree that this dwarf quenched relatively recently (t_{90}) and is thus likely a recent addition to the NGC4826 system. Ancient SFH is highly uncertain and not shown.

Fitting of HST CMDs (Fig 3) is a widely used technique that has successfully recovered the SFHs and quenching times of low-mass dwarfs both inside (e.g. [67, 68, 69, 70]) and outside (e.g. [71, 72, 73, 74]) the LG. The quenching times of satellites in the LG appears to correlate with with known past accretion events (e.g. the infall of the LMC and Gaia-Enceladus [75]). Thus, a uniform census of quenching times of satellites, even at relatively poor temporal resolution, would provide a new means of constraining the build-up of MW-like systems over time; a process that ΛCDM counter-intuitively predicts should produce an anti-correlation between system age and stellar halo mass [76, 77, 78]. HCNS will provide an unprecedented sample of **77 satellites in 5 MW-like systems** (within 5 Mpc) **with uniformly determined SFHs and quenching times**, which will test this prediction and place the LG in context. Although many of these satellites have archival HST observations, these are systematically biased against the fainter satellites that are more likely to have quenched. Both GO and AR components are essential to building a reliable census.

For the satellites in systems beyond 5 Mpc, the photometric depth of the CMDs is unlikely to be deep enough to determine accurate SFHs. For these objects we will instead compare the recent (past ∼300 Myr) SFR to the lifetime average SFR, a technique that has been successfully exploited for low-mass dwarfs out to >10 Mpc with single-orbit observations [73]. This will allow us to robustly separate quenched satellites from those with recent SF, even if that SF was long enough ago that it would not be evident in Hα or UV imaging.

Summary: We propose a 149-orbit Treasury program to perform a volume-limited ($M_{\rm V} < -9$) **census of all satellites around MW-like hosts within 10 Mpc**. This legacy data set will mark a new precision era for small-scale constraints on ΛCDM simulations, with far-reaching implications for our understanding of the evolution and hierarchical growth of MW-like systems, as well as our knowledge of the internal structure of low-mass DM halos.

Description of the Observations

New and archival observations will be reduced and analyzed in the same manner, resulting in a final, uniform data set of 260 color images, photometric catalogs, distance estimates, SFH fits, and GC candidate catalogs, which will be preserved as a HLSP on MAST.

TRGB distances: Identifying the well-calibrated (e.g. [79]) TRGB standard candle through resolved RGB stars is our most observationally demanding science goal. At 10 Mpc the TRGB occurs at $m_{\rm F814W} \approx 26.0$. A $m_{\rm F814W} = 26.0$ star can be detected in F814W with S/N > 4.5 with 2×720 s exposures with UVIS (WFC3UVIS.im.1958088). In this case we will be able to trace the RGB down to at least $m_{\rm F814W} = 26.5$ (at S/N ≥ 3). We will use slightly shorter exposures (2×450 s) in F606W, which at the TRGB will give S/N ≈ 5.0. This represents the **most distant targets** in our sample, thus the vast majority of our observations will trace much further down the RGB. Similar observations have been used to determine TRGB distances to numerous low-mass dwarf galaxies out to 10 Mpc and beyond (e.g. [19, 73, 17]). WFC3 is preferred over ACS due lack of future calibration updates and the fact that ACS is now shared risk. F606W+F814W offer excellent throughput and allow direct comparison to most of the existing related work. HST is best-suited to this project due to the large target sample and the considerable slew overheads of JWST.

Each target in this program has estimated total observing times as follows: 6.5 min for guide star acquisition, 2×2.6 min overhead for 1st exposure in each filter, 2×18 s for dithers, 2×2.1 min overhead for 2nd exposure in each filter, and 2340 s exposure time (both filters combined). This matches the $\sim$49 min allowed per orbit for large programs. Thus, we request 149 orbits, 1 for each new target. Images will be analyzed using `DOLPHOT` [80] and all point-like sources extracted simultaneously from all exposures of each target, allowing us to make use of even low S/N sources in individual exposures. The TRGB location will be measured as in [44], who compare the observed RGB LF to a model LF convolved with the photometric uncertainties and incompleteness computed via artificial star tests.

Star formation histories: SFHs will be fit based on the CMD of each target using a `Python` adaptation of `StarFISH` [81] (used in Fig. 3). As with other CMD-based SFH codes, this performs a maximum likelihood fit to the observed CMD with linear combinations of mock single stellar populations that span a grid of ages and metallicities, accounting for photometric uncertainties and incompleteness. This approach is well-established [81, 82, 83] and has been implemented to recover the SFHs of many dwarf galaxies in the Local Volume (e.g. [71]). One of the products of this Treasury program will be the public release on `github` of our SFH code. We note that this is the only such code based in `Python` of which we are aware and that the SFH code used for most HST/JWST programs remains proprietary [82].

Globular clusters: Even the faintest GCs are much brighter than the TRGB and will be detected at high S/N. This is essential as the galaxies in question are expected to host relatively few GCs. HST is vastly superior to ground-based imaging for identifying GCs and in discriminating them from background objects (e.g. [84]). Most GCs will be at least marginally resolved, further aiding clean selection via profile fitting. We will use both standard background subtraction and a Bayesian mixture approach to assess the number and extent of the GC systems of individual galaxies (where sufficient GCs are identified) and average values for galaxies in stellar mass bins, from which we will recover the GCLF as a function of galaxy stellar mass for low-mass satellites. About 96% of our targets are compact enough that they can be imaged out to 2 half-light radii within the UVIS FoV. The largest targets will require a small statistical correction to their counts for the missing area.

Special Requirements

Minor ORIENT constraints for some targets are needed to avoid nearby bright stars or galaxies.

Coordinated Observations

We have decided not to request parallel observations partly because of the infeasibility of buffer dumps for two instruments, each with two exposures in two filters, in a 49 min period. Accommodating all these dumps is not possible without severely impacting the quality of our primary exposures. Approximately 80% of our targets fit (out to two half-light radii) within a single UVIS chip and the other chip can be used to characterize background/contaminant rates (primarily for the GC search). For the remaining $\sim$20% of our targets we will use the sky regions of the other science fields in the same host system to determine the contaminant rates.

Justify Duplications

A number of our target are in common with the Cycle 32 program SNAP-17797. We have removed any targets that have already been observed in Cycle 32 and if this proposal is accepted we would remove those with successful SNAP observations in the remainder of Cycle 32. However, any of these common targets that have not been observed by the beginning of Cycle 33 should remain in this GO project to ensure that they are observed. Our science relies strongly on there being a complete set of observations for the entire sample, which the SNAP will not provide. We note that the data from HCNS will have no exclusive access period and the SNAP-17797 team will therefore get immediate access to the data for all of their targets that are in common with this proposal when they are observed in Cycle 33.

References

[1] Klypin, A., Kravtsov, A. V., Valenzuela, O., & Prada, F. 1999, ApJ, 522, 82

[2] de Blok, W. J. G. 2010, Advances in Astronomy, 2010, 789293

[3] Bullock, J. S. & Boylan-Kolchin, M. 2017, ARA&A, 55, 343

[4] Sales, L. V., Wetzel, A., & Fattahi, A. 2022, Nature Astronomy, 6, 897

[5] Pawlowski, M. S. 2018, Modern Physics Letters A, 33, 1830004

[6] Karunakaran, A., Sand, D. J., Jones, M. G., et al. 2023, MNRAS, 524, 5314

[7] Geha, M., Wechsler, R. H., Mao, Y.-Y., et al. 2017, ApJ, 847, 4

[8] Mao, Y.-Y., Geha, M., Wechsler, R. H., et al. 2021, ApJ, 907, 85

[9] Carlsten, S. G., Greene, J. E., Peter, A. H. G., Beaton, R. L., & Greco, J. P. 2021, ApJ, 908, 109

[10] Carlsten, S. G., Greene, J. E., Beaton, R. L., Danieli, S., & Greco, J. P. 2022, ApJ, 933, 47

[11] Dalcanton, J. J., Williams, B. F., Seth, A. C., et al. 2009, ApJS, 183, 67

[12] Geha, M., Mao, Y.-Y., Wechsler, R. H., et al. 2024, ApJ, 976, 118

[13] Bennet, P., Sand, D. J., Crnojević, D., et al. 2020, ApJL, 893, L9

[14] Karunakaran, A., Spekkens, K., Carroll, R., et al. 2022, MNRAS, 516, 1741

[15] Deason, A. J., Fattahi, A., Frenk, C. S., et al. 2020, MNRAS, 496, 3929

[16] Mao, Y.-Y., Geha, M., Wechsler, R. H., et al. 2024, ApJ, 976, 117

[17] McQuinn, K. B. W., Telidevara, A. K., Fuson, J., et al. 2021, ApJ, 918, 23

[18] Carlsten, S. G., Greene, J. E., Greco, J. P., Beaton, R. L., & Kado-Fong, E. 2021, ApJ, 922, 267

[19] Cohen, Y., van Dokkum, P., Danieli, S., et al. 2018, ApJ, 868, 96

[20] Bennet, P., Sand, D. J., Crnojević, D., et al. 2019, ApJ, 885, 153

[21] Smercina, A., Bell, E. F., Samuel, J., & D'Souza, R. 2022, ApJ, 930, 69

[22] Mutlu-Pakdil, B., Sand, D. J., Crnojević, D., et al. 2024, ApJ, 966, 188

[23] Pawlowski, M. S. 2021, Galaxies, 9, 66

[24] Sawala, T., Cautun, M., Frenk, C., et al. 2023, Nature Astronomy, 7, 481

[25] Brainerd, T. G. & Samuels, A. 2020, ApJL, 898, L15

[26] Wang, P., Libeskind, N. I., Pawlowski, M. S., et al. 2021, ApJ, 914, 78

[27] Samuels, A. & Brainerd, T. G. 2023, ApJ, 947, 56

[28] Chiboucas, K., Jacobs, B. A., Tully, R. B., & Karachentsev, I. D. 2013, AJ, 146, 126

[29] Ibata, R. A., Lewis, G. F., Conn, A. R., et al. 2013, Nature, 493, 62

[30] Müller, O., Pawlowski, M. S., Jerjen, H., & Lelli, F. 2018, Science, 359, 534

[31] Martínez-Delgado, D., Makarov, D., Javanmardi, B., et al. 2021, A&A, 652, A48

[32] Brodie, J. P. & Strader, J. 2006, ARA&A, 44, 193

[33] Forbes, D. A., Bastian, N., Gieles, M., et al. 2018, Proceedings of the Royal Society of London Series A, 474, 20170616

[34] Reina-Campos, M., Trujillo-Gomez, S., Deason, A. J., et al. 2022, MNRAS, 513, 3925

[35] Reina-Campos, M., Keller, B. W., Kruijssen, J. M. D., et al. 2022, MNRAS, 517, 3144

[36] Doppel, J. E., Sales, L. V., Nelson, D., et al. 2023, MNRAS, 518, 2453

[37] Peng, E. W., Jordán, A., Côté, P., et al. 2006, ApJ, 639, 95

[38] Jordán, A., McLaughlin, D. E., Côté, P., et al. 2007, ApJS, 171, 101

[39] Villegas, D., Jordán, A., Peng, E. W., et al. 2010, ApJ, 717, 603

[40] Cho, J., Sharples, R. M., Blakeslee, J. P., et al. 2012, MNRAS, 422, 3591

[41] Floyd, M., Chandar, R., Whitmore, B. C., et al. 2024, AJ, 167, 95

[42] Saifollahi, T., Voggel, K., Lançon, A., et al. 2024, arXiv e-prints, arXiv:2405.13500

[43] Carlsten, S. G., Greene, J. E., Beaton, R. L., & Greco, J. P. 2022, ApJ, 927, 44

[44] Crnojević, D., Sand, D. J., Bennet, P., et al. 2019, ApJ, 872, 80

[45] Spitler, L. R., Forbes, D. A., Strader, J., Brodie, J. P., & Gallagher, J. S. 2008, MNRAS, 385, 361

[46] Harris, W. E., Harris, G. L. H., & Alessi, M. 2013, ApJ, 772, 82

[47] Zaritsky, D., Crnojević, D., & Sand, D. J. 2016, ApJL, 826, L9

[48] Forbes, D. A., Read, J. I., Gieles, M., & Collins, M. L. M. 2018, MNRAS, 481, 5592

[49] Miller, B. W. & Lotz, J. M. 2007, ApJ, 670, 1074

[50] Eadie, G. M., Harris, W. E., & Springford, A. 2022, ApJ, 926, 162

[51] Goerdt, T., Moore, B., Read, J. I., Stadel, J., & Zemp, M. 2006, MNRAS, 368, 1073

[52] Amorisco, N. C. 2017, ApJ, 844, 64

[53] Strigari, L. E., Bullock, J. S., Kaplinghat, M., et al. 2006, ApJ, 652, 306

[54] Nipoti, C., Ciotti, L., Binney, J., & Londrillo, P. 2008, MNRAS, 386, 2194

[55] Yozin, C. & Bekki, K. 2012, ApJL, 756, L18

[56] Cole, D. R., Dehnen, W., Read, J. I., & Wilkinson, M. I. 2012, MNRAS, 426, 601

[57] Amorisco, N. C., Agnello, A., & Evans, N. W. 2013, MNRAS, 429, L89

[58] Meadows, N., Navarro, J. F., Santos-Santos, I., Benítez-Llambay, A., & Frenk, C. 2020, MNRAS, 491, 3336

[59] Genina, A., Read, J. I., Fattahi, A., & Frenk, C. S. 2022, MNRAS, 510, 2186

[60] Spekkens, K., Urbancic, N., Mason, B. S., Willman, B., & Aguirre, J. E. 2014, ApJL, 795, L5

[61] Putman, M. E., Zheng, Y., Price-Whelan, A. M., et al. 2021, ApJ, 913, 53

[62] Cortese, L., Catinella, B., & Smith, R. 2021, PASA, 38, e035

[63] Karunakaran, A., Spekkens, K., Oman, K. A., et al. 2021, ApJL, 916, L19

[64] Bressan, A., Marigo, P., Girardi, L., et al. 2012, MNRAS, 427, 127

[65] Dotter, A. 2016, ApJS, 222, 8

[66] Hidalgo, S. L., Pietrinferni, A., Cassisi, S., et al. 2018, ApJ, 856, 125

[67] Weisz, D. R., Dolphin, A. E., Skillman, E. D., et al. 2014, ApJ, 789, 147

[68] Weisz, D. R., Martin, N. F., Dolphin, A. E., et al. 2019, ApJL, 885, L8

[69] Savino, A., Weisz, D. R., Skillman, E. D., et al. 2023, ApJ, 956, 86

[70] Savino, A., Weisz, D. R., Dolphin, A. E., et al. 2025, ApJ, 979, 205

[71] Weisz, D. R., Dalcanton, J. J., Williams, B. F., et al. 2011, ApJ, 739, 5

[72] Cole, A. A., Weisz, D. R., Dolphin, A. E., et al. 2014, ApJ, 795, 54

[73] McQuinn, K. B. W., Cannon, J. M., Dolphin, A. E., et al. 2015, ApJ, 802, 66

[74] Hargis, J. R., Albers, S., Crnojević, D., et al. 2020, ApJ, 888, 31

[75] D'Souza, R. & Bell, E. F. 2021, MNRAS, 504, 5270

[76] D'Souza, R. & Bell, E. F. 2018, MNRAS, 474, 5300

[77] D'Souza, R. & Bell, E. F. 2018, Nature Astronomy, 2, 737

[78] Harmsen, B., Bell, E. F., D'Souza, R., et al. 2023, MNRAS, 525, 4497

[79] Jang, I. S. & Lee, M. G. 2017, ApJ, 835, 28

[80] Dolphin, A. E. 2000, PASP, 112, 1383

[81] Harris, J. & Zaritsky, D. 2001, ApJS, 136, 25

[82] Dolphin, A. E. 2002, MNRAS, 332, 91

[83] Hidalgo, S. L., Aparicio, A., Skillman, E., et al. 2011, ApJ, 730, 14

[84] Côté, P., Blakeslee, J. P., Ferrarese, L., et al. 2004, ApJS, 153, 223